PEDIATRICS INTERNATIONAL Official Journal of the Japan Pediatric Society

Pediatrics International (2013) **55**, e103–e106 doi: 10.1111/ped.12098

Patient Report

Case of an infant with hepatic cirrhosis caused by mitochondrial respiratory chain disorder

Shigehiro Enkai,[1] Sachi Koinuma,[2] Reiko Ito,[2] Junko Igaki,[3] Yukihiro Hasegawa,[3] Kei Murayama[4] and Akira Ohtake[5]

[1]*Department of Pediatrics, Fussa Hospital,* [2]*Division of Gastroenterology, National Center for Child Health and Development,* [3]*Division of Endocrinology and Metabolism, Tokyo Metropolitan Children's Medical Center, Tokyo,* [4]*Division of Metabolism, Chiba Children's Hospital, Chiba, and* [5]*Department of Pediatrics, Faculty of Medicine, Saitama Medical University, Saitama, Japan*

Abstract The patient had hepatomegaly with liver dysfunction at the age of 1 month. Magnetic resonance imaging performed at the age of 1 year showed multiple nodules of varying size in his liver. We were able to examine the mitochondrial respiratory chain function in the liver biopsy samples because all other differential diagnoses for hepatic cirrhosis had been ruled out. Complex I and IV activities were below the normal level (<30%) of the citrate synthase (CS) ratio. Liver blue native polyacrylamide gel electrophoresis showed an extremely weak complex I and IV band. Liver respiratory chain complexes I and IV were found to be deficient in this patient. The histologic findings were highly suggestive of mitochondrial respiratory chain disorder. Findings of progressive liver cirrhosis changes were observed in magnetic resonance imaging at the age of 5 years. An examination of the mitochondrial respiratory chain function should be performed along with a liver biopsy if mitochondrial respiratory chain disorder is suspected as a possible differential diagnosis of idiopathic hepatitis.

Key words chronic hepatitis, infant, liver cirrhosis, mitochondrial respiratory chain complex I and IV deficiency, mitochondrial respiratory chain disorder.

Mitochondrial respiratory chain disorder (MRCD), which is caused by the loss of one or more enzyme activities in respiratory chain complexes I–IV, has many clinical manifestations in various organs and is a known cause of mitochondrial encephalomyopathy, idiopathic hepatitis and idiopathic muscle weakness. Although MRCD is one of the differential diagnoses for hepatic disorder, it is not actively diagnosed. The early diagnosis of MRCD in the liver is important because some patients will subsequently develop liver cirrhosis or liver failure.[1,2] This report is based on a boy with chronic hepatic disorder and cirrhosis who was found to have mitochondrial respiratory chain complex I and IV deficiencies during his infant period.

Case Report

The patient was a Japanese boy born at term and weighing 3296 g; he was the second child of healthy parents with consanguinity. His elder sister (3 years old) is presently in good health. The mother's brother (31 years old) was found to have hepatic dysfunction during his infant period and his condition progressed to cirrhosis during adulthood. The proband's weight gain after birth was good. Jaundice and hepatomegaly were observed at the age of 1 month and he was admitted to our hospital. Upon admission (32 days after birth), he exhibited conjunctival icterus, his liver was palpable 5 cm below the right costal margin, he had normal muscle tone and no external malformations were noted. His laboratory data on admission showed cholestatic hepatitis. Tandem mass spectrometry, urine organic acid and bile acid analysis were normal. The following differential diagnoses were ruled out: autoimmune disease, infectious disease, disorder of organic acid metabolism and fatty acid oxidation, alpha 1-antitrypsin deficiency, tyrosinemia, galactosemia, and citrin deficiency. Furthermore, respiratory disorder, abnormal findings on skin or bone, and susceptibility to infection, which are the main symptoms of Langerhans cell histiocytosis and cystic fibrosis, are not present in this patient at the current age of 6 years. Imaging studies did not reveal any congenital portal venous or portal biliary tract malformations. The patient's transaminase (aspartate aminotransferase [AST] and alanine aminotransferase [ALT]) levels were 78–477 IU/l (AST) and 13–181 IU/l (ALT) and fluctuated with his physical condition. The patient's γ-GTP levels decreased to a normal range before the age of 6 months. Throughout the clinical course, the patient's blood lactate and pyruvic acid levels were almost always normal. Hypoglycemia was not observed during follow-up examinations. He exhibited normal growth and development. An abdominal magnetic resonance imaging (MRI) examination performed at the age of 2 months was normal except for hepatomegaly. However, an abdominal MRI performed at 1 year and 4 months showed multiple nodules of varying size in his liver, which appeared

Correspondence: Shigehiro Enkai, MD, Department of Pediatrics, Fussa Hospital, 1-6-1 Kamidaira, Fussa, Tokyo 197-0012, Japan. Email: enkai@fussahp.jp

Received 5 January 2012; revised 17 January 2013; accepted 19 February 2013.

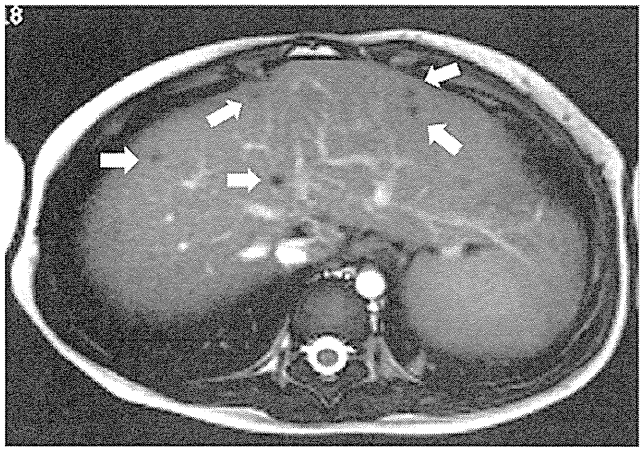

Fig. 1 Abdominal magnetic resonance image obtained at 1 year and 4 months shows multiple nodules (arrows) varying in size in the liver, which presented as a low-intensity area on T2-weighted imaging.

as low-intensity areas on T2-weighted images (see Fig. 1) and high-intensity areas on T1-weighted images without contrast enhancement. The number of nodules in his liver increased from the time of the MRI examination performed at the age of 1 year and 4 months. In addition, a transient elevation in the patient's serum ammonia levels (290 μg/dL) and impaired consciousness with the onset of fever and a poor appetite were observed at the age of 2 years. The clinical course during this episode showed positive results. Liver biopsies were performed during a laparotomy to inspect the progress of the liver cirrhosis at the age of 2 years and 1 month. He was suspected of having MRCD, which is one of the main causes of hepatic disorder, because all other differential diagnoses for hepatic cirrhosis had been ruled out. Thus, we were able to examine the mitochondrial respiratory chain function in the liver biopsy samples. Liver respiratory chain complexes I and IV were found to be deficient in this patient using both a respiratory chain enzyme assay (Table 1) and a liver blue native polyacrylamide gel electrophoresis (BN-PAGE).[3] Complex I and IV activities were below the normal level (<30%)[4] of the CS ratio. Liver BN-PAGE showed an extremely weak complex I and IV band in this patient. In addition, the rate of mtDNA and nDNA (quantitative polymerase chain reaction) was about 95.4% (normal level). Mitochondrial DNA depletion syndrome was ruled out. The macroscopic anatomy showed diffuse nodules on the surface of the liver. The microscopic findings for the liver are shown in Figure 2. Coenzyme Q, vitamin C, vitamin E, and carnitine therapy were initiated at an age of 2 years and 3 months. The patient continues to exhibit normal physical and mental development after diagnosis. His weight was 21.9 kg (+0.3SD score) and height was 117.5 cm (+0.6SD score) at the age of 6 years. However, the patient's transaminase levels were 56–311 IU/L (AST) and 31–174 IU/L (ALT), and findings of the follow-up MRI at the age of 5 years suggested progressive changes in liver cirrhosis. MRI demonstrated right lobe atrophy, enlargement of the left lobe, and an irregular edge border of the liver (Fig. 3a,b). MRI revealed a well-circumscribed mass 16 × 11-mm (see arrow) in liver segment VI (Fig. 3c). In addition to this mass, MRI demonstrated nodules 4–8 mm in size in the liver parenchyma, which were visualized as slightly hyperintense lesions on the T2-weighted images and as hypointensities on the T1-weighted images (Fig. 3c).

Table 1 Respiratory chain enzyme assay in the liver of the patient

	Complex I	Complex II	Complex III	Complex IV	CS
% of normal	14	37	62	15	54
CS ratio (%)	26	67	111	27	
Complex II ratio (%)	38		165	40	

Discussion

We reported a boy with chronic hepatic disorder and cirrhosis who was found to have mitochondrial respiratory chain complex I and IV deficiency during his infant period. In our experience, deficiencies of complexes I and IV account for about 15% of all diagnosed cases of MRCD in Japanese subjects. Nine clinical case reports of complex I and IV deficiencies, including adult subjects, were reported between 1988 and 2010. No specific manifestations of complex I and IV deficiency were observed in the past reports. The patient's blood lactate/pyruvate rate was almost normal in the clinical course. However, a normal lactate level does not exclude respiratory chain defects in MRCD, including mitochondrial hepatopathy.[5,6] The molecular and genetic causes of complex I and IV deficiency are not clear.

The histological findings of liver biopsy specimens from patients with primary mitochondrial hepatopathies reveal individual, non-specific histologic and ultrastructural findings, with predominant microvesicular steatosis and canalicular cholestasis.[7] Periportal and centrilobular fibrosis are characteristic features, and the dropout of broad bands of hepatocytes leads to micronodular cirrhosis.[7] Thus, the histologic findings of this case were highly suggestive of MRCD. In addition, if electron micrographs revealed morphological abnormality of mitochondria in liver biopsies, they would have been useful for confirming diagnosis of MRCD.

With respect to MRI findings, nodules which were found at the age of 1 year were not detected at the age of 5 years. The nodules in Figure 1 might be regenerative nodules (RN) associated with hepatic cirrhosis, because RN typically appear as hypointense lesions on T2-weighted images[8] and the imaging findings at the age of 5 years were typical of hepatic cirrhosis. Furthermore, focal nodular hyperplasia, which is one of the important differential diagnoses of hepatic nodules in infants, was excluded on the basis of the high signal intensity in the non-enhanced T2-weighted images.[9] However, these nodules were so small that they were difficult to evaluate by MRI or histopathology.

Findings of progressive liver cirrhosis changes were observed in a liver MRI at the age of 5 years (Fig. 3a–c). The 16 × 11-mm mass in Figure 3c (see arrow) was visualized as a hyperintensity on opposed-phase T1-weighted gradient-echo images and as a slightly low-intensity area on the T2-weighted images. Focal

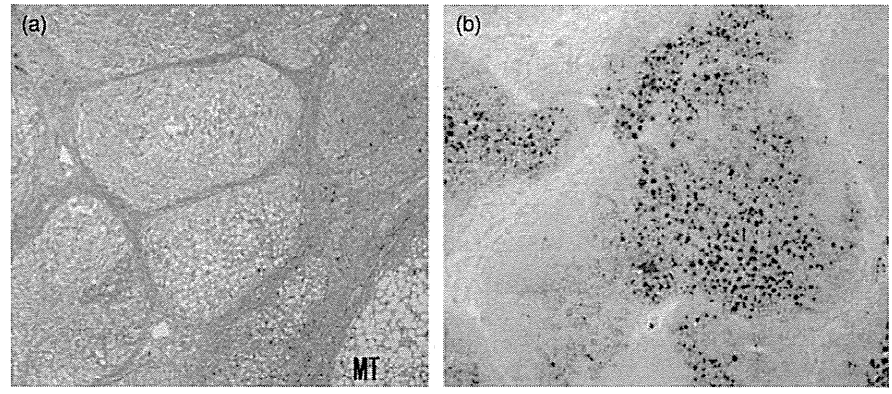

Fig. 2 (a) Masson trichrome stain: Microscopic findings in the liver show the division of a hepatic lobule into nodules by bridging fibrosis in the liver tissue. (b) Sudan III stain: Liver tissues show heterogeneous hepatic steatosis in each septum. Portal fibrosis was observed in liver tissues without inflammation (not shown).

nodular hyperplasia was excluded because the mass did not show the high-intensity on the non-enhanced T2-weighted images. The size remained unchanged as compared to the previous year. Thus, the mass was suspected to be a regenerative nodule or adenomatous hyperplasia, associated with hepatic cirrhosis. In addition to this mass, MRI in Figure 3c demonstrated nodules 4–8 mm in size in the liver parenchyma. Although these nodules were found to contain lipids inside, as they were visualized as low-intensity areas on opposed-phase T1-weighted gradient-echo images and as high-intensity areas on in-phase images, they were too small to evaluate in detail.

The early and accurate diagnosis of MRCD is important because appropriate therapy and guidance can be provided to the patient and his/her family before the condition worsens. MRCD is difficult to diagnose because the clinical manifestations do not depend on the type of complex deficiency. Some previous patients have died of hepatic failure during the neonatal period or infancy, while other patients never develop hepatic disease despite long-term follow-up observation.[1] However, it is conceivable that a regular screening for secondary liver cancer is necessary for the patient with progressive cirrhosis, along with MRCD during his infant period.[10]

With respect to diagnosis, regular ultrasound or CT examinations are needed for infants with idiopathic chronic hepatitis because multiple nodules in the liver gradually appeared in the patient. Furthermore, we conclude that an examination of the mitochondrial respiratory chain function should be performed along with a liver biopsy if MRCD is suspected as a possible differential diagnosis of idiopathic hepatitis under the signs of liver cirrhosis, as in this case.

Acknowledgments

The authors report no conflicts of interest. We have no disclosures to make and have not received any financial support.

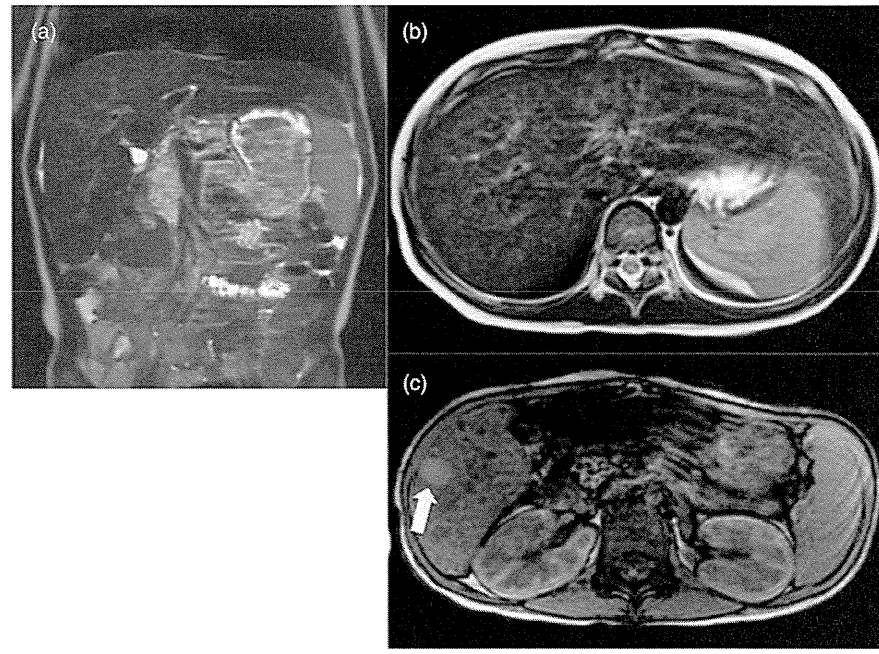

Fig. 3 (a) T2-weighted magnetic resonance image (MRI) demonstrates right lobe atrophy, enlargement of the left lobe, and an irregular edge border of the liver at the age of 5 years. (b) T2-weighted MRI shows marked hyperintensity in the periportal region. The hepatic parenchyma appears heterogeneously enhanced in the delayed phase. (c) T1-weighted MRI revealing a well-circumscribed 16 × 11-mm mass (see arrow) in liver segment VI. This mass is visualized as a hyperintensity on opposed-phase T1-weighted gradient-echo images and as a slightly lower-intensity area on the T2-weighted images. In addition to this mass, MRI demonstrates nodules 4–8 mm in size in the liver parenchyma, which are visualized as slightly hyperintense lesions on the T2-weighted images and as hypointensities on the T1-weighted images.

References

1 Carcia-cazorla A, De Lonlay P, Rustin P *et al.* Mitochondrial respiratory chain deficiencies expressing the enzymatic deficiency in the hepatic tissue: a study of 31 patients. *J. Pediatr.* 2006; **149**: 401–5.
2 Lee WS, Sokol RJ. Mitochondrial hepatopathies: advances in genetics and pathogenesis. *Hepatology* 2007; **45**: 1555–65.
3 Schagger H, Aquila H, von Jagow G. Coomassie blue-sodium dodecyl sulfate- polyacrylamide gel electrophoresis for direct visualization of polypeptides during electrophoresis. *Anal. Biochem.* 1988; **173**: 201–55.
4 Bernier FP, Boneh A, Dennett X, Chow CW, Cleary MA, Thorburn DR. Diagnostic criteria for respiratory chain disorders in adults and children. *Neurology* 2002; **59**: 1406–11.
5 Kirby MD, Crawford M, Cleary MA, Dahl HH, Dennet X, Thorburn DR. Respiratory chain complex I deficiency: an underdiagnosed energy generation disorder. *Neurology* 1999; **52**: 1255–64.
6 Fellman V, Kotarsky H. Mitochondrial hepatopathies in the newborn period. *Semin. Fetal Neonatal Med.* 2011; **16**: 222–8.
7 Suchy FJ, Sokol RJ, Balistreri WF. *Liver Disease in Children*, 3rd edn. Cambridge University Press, Cambridge, 2007; 803–29.
8 Hussain SM, Terkivatan T, Zondervan PE *et al.* Focal nodular hyperplasia: Findings at state-of-the-art MR imaging, US, CT, and pathologic analysis. *Radiographics* 2004; **24**: 3–17.
9 Hanna RF, Aguirre DA, Kased N, Emery SC, Peterson MR, Sirlin CB. Cirrhosis-associated hepatocellular nodules: correlation of histopathologic and MR imaging features. *Radiographics* 2008; **28**: 747–69.
10 Scheers I, Bachy V, Stephenne X, Sokal EM. Risk of hepatocellular carcinoma in liver mitochondrial respiratory chain disorders. *J. Pediatr.* 2005; **146**: 414–7.

Endoplasmic Reticulum Stress and Apoptosis Contribute to the Pathogenesis of Dominantly Inherited Isolated GH Deficiency Due to *GH1* Gene Splice Site Mutations

Daisuke Ariyasu, Hiderou Yoshida,* Makoto Yamada, and Yukihiro Hasegawa*

Department of Endocrinology and Metabolism (D.A., Y.H.), Tokyo Metropolitan Children's Medical Center, Tokyo 183–8561, Japan; Department of Biochemistry and Molecular Biology (H.Y.), Graduate School of Life Science, University of Hyogo, Hyogo 678–1297, Japan; and Department of Pharmacy (M.Y.), Tokyo University of Science, Tokyo 162–0825, Japan

Dominantly inherited isolated GH deficiency is mainly caused by a heterozygous donor site mutation of intron 3 in the *GH1* gene. An exon 3 deletion in GH (del32–71 GH) is produced from a mutant allele, whereas wild-type GH is produced from the other allele. Several studies have demonstrated a dominant negative effect of del32–71 GH on wild-type GH secretion, but the precise molecular mechanisms remain unclear. We hypothesized that unfolded del32–71 GH accumulates in the endoplasmic reticulum (ER) and causes ER stress and apoptosis in somatotrophs, promoting GH deficiency. To evaluate del32–71 GH–mediated ER stress, we established GH4C1 cell lines with doxycycline (dox)-controlled del32–71 GH expression. In 20 of 23 dox-controlled cell lines, the concentration of wild-type GH in the culture medium significantly decreased with del32–71 GH induction, demonstrating the dominant negative effect of this mutant. Cell viability, mRNA abundance of ER stress-response genes, caspase activation, and DNA fragmentation were evaluated in 5 dox-controlled cell lines selected as cellular models. In 4 of the 5 cell lines, del32–71 GH induction decreased cell viability, increased expression of 3 major ER stress response pathways (PRKR-like endoplasmic reticulum kinase [PERK], activating transcription factor-6 [ATF6], and inositol requirement 1 [IRE1]), and induced caspase-3 and caspase-7 activation. In 1 of the 4 cell lines, DNA fragmentation was demonstrated. Finally, overexpression of XBP1(S), a nuclear transcription factor downstream of IRE1, completely reversed the observed caspase activation. These data suggested that del32–71 GH–mediated ER stress and apoptosis contributed to the decrease in wild-type GH secretion observed in GH deficiency due to the *GH1* gene slice-site mutations. (***Endocrinology* 154: 3228–3239, 2013**)

Dominantly inherited isolated GH deficiency is mainly caused by heterozygous donor-site mutations of intron 3 in the *GH1* gene (1, 2). Such splice-site mutations cause in-frame mRNA skipping of exon 3, corresponding to amino acids 32 to 71. As a result, a 17.5-kDa exon 3 deletion-mutant GH protein (del32–71 GH) is produced from the mutant allele. The GH transcript from the other wild-type allele includes exons 1 to 5 and produces a 22-kDa wild-type GH protein. One wild-type *GH1* allele appears to be sufficient to maintain a serum concentration of wild-type GH within the normal range because children harboring a deletion in just one *GH1* allele exhibit a normal stature (3). However, patients with the splice-site mutations have low serum concentrations of wild-type GH, despite the presence of one wild-type *GH1* gene. Thus, it has been suggested that del32–71 GH exerts a dominant negative effect on the secretion of wild-type GH, but the precise molecular mechanisms involved have remained

ISSN Print 0013-7227 ISSN Online 1945-7170
Printed in U.S.A.

Received March 17, 2013. Accepted May 29, 2013.
First Published Online June 4, 2013

* H.Y. and Y.H. contributed equally to the study.

Abbreviations: ATF6, activating transcription factor-6; dox, doxycycline; EM, electron microscopy; ER, endoplasmic reticulum; ERAD, endoplasmic reticulum–associated degradation; IRE1, inositol requirement 1; IRMA, immunoradiometric assay; PERK, PRKR-like endoplasmic reticulum kinase; q, quantitative.

elusive. It has been speculated that del32–71 GH lacks the loop connecting helix 1 and helix 2 (4), and, therefore, the protein cannot be properly folded in the endoplasmic reticulum (ER) (5, 6). In addition, one study has shown that unfolded del32–71 GH interferes with the wild-type GH secretory pathway by destroying secretory vesicles (7).

Proteins are synthesized and folded in the ER, and only correctly folded proteins are transported to the Golgi apparatus. Proteins judged as "unfolded" in the ER are (1) suppressed at the translational level, (2) refolded by ER chaperones, or (3) degraded by the proteasome via endoplasmic reticulum–associated degradation (ERAD) machinery. In mammals, these 3 cell-protective responses are executed through the PRKR-like endoplasmic reticulum kinase (PERK), activating transcription factor-6 (ATF-6), and inositol requirement 1 (IRE1) pathways, respectively (8–11). These self-defense mechanisms in eukaryotic cells, which function to alleviate the stress caused by unfolded proteins, are collectively referred to as the ER stress responses. When cells synthesize unfolded proteins in amounts that exceed the capacity of the self-defense mechanisms, an apoptotic pathway is triggered to ensure survival of the organism as the last line of defense (12). ER stress has a significant role in the development of several diseases, such as Alzheimer disease, Parkinson disease, type 2 diabetes, familial central diabetes insipidus, and Wolfram syndrome (13–18).

Based on these previous studies, we hypothesized that ER stress, caused by unfolded del32–71 GH accumulating in the ER, may be one of the factors involved in the development of GH deficiency due to the splice site mutations. Involvement of ER stress in the dominant negative effect of del32–71 GH has been speculated to be unlikely in 2 studies (5, 7). However, these 2 studies did not evaluate ER stress using cells expressing both human wild-type and del32–71 GH; the former study (5) performed transient expression of del32–71 GH to COS cells, and the latter study (7) stably expressed del32–71 GH to rat GC cells. Thus, we tried to analyze the involvement of ER stress using cells stably expressing human wild-type and del32–71 GH.

In this study, in vitro data indicated that del32–71 GH caused ER stress and apoptosis in GH4C1 rat pituitary cells. Using a doxycycline (dox)-inducible gene expression system, we established double-transfected stable GH4C1 cell lines in which wild-type GH was constantly expressed and del32–71 GH expression was induced. Using 5 cell lines chosen as a cellular model of this disorder, we demonstrated that the induction of del32–71 GH caused ER stress, leading to apoptosis of the cells.

Materials and Methods

Isolation of wild-type GH1 cDNA and del32–71 GH1 cDNA

Wild-type and del32–71 GH1 cDNA sequences were amplified from a pituitary cDNA library by standard PCR methods using a sense primer that includes the initiation codon and an antisense primer that includes the termination codon. The initial PCR product was subjected to electrophoresis on a 1% agarose gel, and regions around 670 and 550 bp, corresponding with the PCR products of wild-type and del32–71 GH1 cDNA, respectively, were separately isolated and purified. The 550-bp PCR product was amplified by a second PCR using the same primers. The second PCR product was purified, and the deletion of exon 3 was confirmed by direct sequencing.

Expression vectors

For preparation of constructs for the dox-inducible gene expression system, we employed the Tet-Off Advanced Doxycycline Inducible Gene Expression System (Clontech Laboratories, Mountain View, California). First, wild-type *GH1* cDNA was inserted into the pcDNA3.1-Hygro(+) vector (Invitrogen, Carlsbad, California) using NheI and ApaI restriction enzymes (pcDNA3.1–wild-type GH). Regions containing the cytomegalovirus promoter, wild-type *GH1* cDNA sequence, and polyadenine signal were isolated from pcDNA3.1–wild-type GH using standard PCR methods and inserted into the Tet-Off Advanced Vector (supplied with the kit) via a HindIII restriction site in the 5′ to 3′ direction (Tet-Off advanced–wild-type GH). del32–71 GH1 cDNA was inserted into the pTRE–Tight Vector (supplied with the kit) via KpnI and HindIII restriction sites (pTRE–del32–71 GH). For preparation of GFP-XBP1(S) expression constructs, the rat *XBP1(S)* cDNA sequence was amplified and purified from mRNA of thapsigargin-treated GH4C1 cells by RT-PCR and inserted into the pTagGFP2-C vector (Evrogen, Moscow, Russia) using XhoI and KpnI restriction enzymes [GFP-XBP1(S)]. All primers sequences used in this study are listed in Supplemental Table 1 published on The Endocrine Society's Journals Online web site at http://endo.endojournals.org.

Cell culture

GH4C1 rat pituitary cells, which are known to secrete little rat GH, were purchased from American Type Culture Collection (Manassas, Virginia). GH4C1 cells were cultured in Ham's F-10 medium, 15% horse serum, and 2.5% fetal bovine serum (both sera were not heat-inactivated). Endogenous rat GH was confirmed to be absent from the culture medium by immunoblotting with human anti-GH antibodies (Dako, Carpinteria, California) and RT-PCR.

Transfection

Lipofectamine reagent (Invitrogen) and Lipofectamine Plus reagent (Invitrogen) were used for transfections. Transfections were performed according to the manufacturer's instructions 48 hours after seeding at a density of 5×10^5 cells per 2 mL of medium in 6-well culture plates.

Establishment of stable cell lines using a dox-inducible gene expression system

GH4C1 cells were transfected with Tet-Off advanced wild-type GH (explained above). Culture medium containing 0.4 mg/mL G418 (Promega, Madison, Wisconsin) was exchanged every 3 days. Each surviving cell line was transiently transfected with pTRE–Tight Luc vector (supplied with the kit) in the presence or absence of 100 ng/mL dox (supplied with the kit), and fold inductions (−dox/+dox) of luciferase activity were calculated. Expression of human wild-type GH and fold induction of luciferase activity were evaluated among all 40 stable cell lines by immunoblotting and luciferase assays, respectively, and only 1 of these 40 cell lines was chosen. Next, the cell line was transfected with pTRE–del32–71 GH and hygromycin marker (supplied with the kit) with a molar ratio of 20:1 in the presence of 100 ng/mL dox. Culture medium containing 100 ng/mL dox, 0.4 mg/mL G418, and 0.2 mg/mL hygromycin (Invitrogen) was exchanged every 3 days. Individual double-transfected stable cell lines were evaluated for expression of wild-type GH and del32–71 GH in the presence or absence of 100 ng/mL dox by quantitative (q) RT-PCR and immunoblotting.

RT-PCR and qRT-PCR

Total RNA (500 ng) was extracted using RNAiso Plus (Takara, Tokyo, Japan) and then converted to cDNA using PrimeScript RT Master Mix (Takara). The aliquot of cDNA was used for RT-PCR and qRT-PCR. A Taq polymerase, KOD-FX (Toyobo, Osaka, Japan), was used for standard PCR and RT-PCR, and SYBR Premix Ex Taq II (Takara) was used for qRT-PCR.

qRT-PCR was performed using a Thermal Cycler Dice Real Time System (Takara). The amplification conditions consisted of 1 cycle at 95°C for 30 seconds and 35 cycles at 95°C for 5 seconds and 60°C for 30 seconds. Dissociation curve analyses were performed at conditions of 95°C for 15 seconds, 60°C for 30 seconds, and 95°C for 15 seconds. The relative concentrations of mRNAs were calculated using the standard curve and normalized to β-actin expression.

Evaluation of ER stress response gene transcript

The relative abundance of ER stress response gene transcripts was evaluated by qRT-PCR. As ER stress response genes, *GADD34*, *CHOP*, *BiP*, *GRP94*, and *XBP1* were chosen in this study. BiP and XBP1 were also used as ER stress markers for the purpose of screening cell lines with dox-controlled del32–71 GH expression. BiP is an ER chaperone downstream of ATF6 that enhances folding capacities in the ER and XBP1 is a transcription factor downstream of IRE1 that activates transcription of ERAD components (12).

SDS-PAGE and immunoblotting

SDS-PAGE and immunoblotting were performed using 15% polyacrylamide gels, polyvinylidene difluoride membranes, and ECL Plus detection reagent (Amersham, Little Chalfont, Buckinghamshire, England) according to standard procedures (19).

In soluble/insoluble fraction assays, cells cultured in 60-mm dishes were scraped, suspended in 50 μL of 1% Triton X-100 in PBS, and incubated at 4°C for 15 min. The lysates were centrifuged at 17 800 *g* for 5 min, and the supernatants and precipitates were isolated in separate microfuge tubes. Next, 16.7 μL of 4× sample buffer (0.1 mM Tris-HCl, pH 6.8, containing 4% SDS, 20% sucrose, 0.01% bromophenol blue, and 10% 2-mercaptoethanol) was added to each supernatant, and 50 μL of radioimmunoprecipitation assay buffer (10 mM Tris-HCl, pH 7.4, containing 5 mM EDTA, 0.1% SDS, and 1% Triton X-100) plus 16.7 μL of 4× sample buffer was added to each precipitate. Supernatants and precipitates were heated at 100°C for 5 minutes and centrifuged at 17 800 *g* for 15 minutes at 4°C. Aliquots of the resulting supernatants were loaded onto 15% polyacrylamide gels.

Measuring the GH concentration in culture medium

Cell lines with dox-controlled del32–71 GH expression were seeded at a density of 2.5×10^4 cells/150 μL of culture medium into 96-well culture plates in the presence or absence of 100 ng/mL dox. Forty-eight hours later, 100 μL of culture medium was collected from each cell line and mixed with 400 μL of PBS. The GH concentration was subsequently measured by a commercially available immunoradiometric assay (IRMA) using a GH measuring kit (Daiichi; TFB, Tokyo, Japan). We confirmed that del32–71 GH was absent from this assay; a concentration of del32–71 GH in MG132-treated near-confluent GH4C1 cell lysates transfected with del32–71 GH was below the detectable limit. The measurement range for IRMA was 0.05 to 25 ng/mL. Both intra- and interassay coefficients of variation were less than 3%.

Cell viability

Cell lines with dox-controlled del32–71 GH expression were seeded at a density of 2.5×10^4 cells/150 μL of medium into 96-well culture plates in the presence or absence of 100 ng/mL dox. Forty-eight hours after seeding, 10% CCK-8 reagent (Dojindo, Kumamoto, Japan) was added with fresh culture medium. Absorbance was measured 4 hours later using a multiplate reader. The CCK-8 reagent contained a water-soluble disulfonated tetrazolium salt that was reduced by NADH to produce the corresponding formazan dye (absorbance at 460 nm). CCK-8 reagent has been used as a chromogenic indicator for NADH and cell viability (20).

DNA fragmentation assay

To assess DNA ladder formation, low–molecular-weight DNA was extracted from 2×10^6 cells using the ApoLadder EX Kit (Takara). Extracted DNA fragments were applied to 2% agarose gels, separated electrophoretically, and visualized with GelRed (Wako Chemicals, Irvine, California).

Reagents for the pharmacological induction of ER stress, proteasome inhibition, and lysosome inhibition

Thapsigargin (Sigma-Aldrich, St Louis, Missouri), the proteasome inhibitor MG132 (Peptide Institute, Osaka, Japan), and chloroquine (Sigma-Aldrich) were added to the culture medium 16 hours before harvesting at final concentrations of 1 μM, 10 μM, and 50 μg/mL, respectively.

Detection of caspase-3 and caspase-7 activation

Cell lines with dox-controlled del32–71 GH expression were seeded at a density of 2.5×10^4 cells/150 μL of culture medium into 96-well culture plates in the presence or absence of 100 ng/mL dox. Six wells for each cell line were visualized using an Image-iT LIVE Red Caspase-3 and -7 Detection Kit (Molecular Probes; Invitrogen) 24 hours after induction. Twenty pictures for each cell line were taken under a fluorescence microscope with ×200 magnification. At least 3800 cells for each cell line were counted, and cells producing luminescence above a certain threshold intensity were judged as caspase-positive using WinROOF (Mitani Corp., Tokyo, Japan). The threshold was kept constant in all cell lines.

Image analysis and statistics

Expression levels of ER stress response genes were statistically evaluated by the Student *t* test. The ratio of caspase-3– and caspase-7–positive cells to total cells under a fluorescence microscope and the ratio of vacuole area to cytosol area under an electron microscope were evaluated using WinROOF and statistically evaluated by a Student *t* test. The ratio of apoptotic cells to surviving cells after overexpression of XBP1(S) was analyzed by the χ^2 test.

Results

Concentrations of wild-type GH secreted in culture media decreased with induction of del32–71 GH

For the purpose of evaluating ER stress caused by del32–71 GH, GH4C1 cell lines with dox-controlled del32–71 GH expression, in which wild-type GH was stably expressed and del32–71 GH expression was induced by removing dox from the culture medium, were established. In the classic stable cell lines established by constructs using a cytomegalovirus promoter, we observed preferential growth of cells resistant to del32–71 GH–induced ER stress, and ER stress responses were presumably diluted after successive culturing. Establishment of these dox-controlled cell lines enabled us to suppress del32–71 GH expression by adding dox continuously into the culture media, thereby minimizing this selection bias. In addition, these cell lines enabled us to evaluate del32–71 GH–induced ER stress by comparing cells in the presence or absence of dox-mediated induction under the same genetic background.

First, concentrations of wild-type GH in culture media were evaluated by IRMA for all 23 dox-controlled cell lines with or without del32–71 GH induction. In 20 of the 23 cell lines, wild-type GH concentrations in the media decreased by 18.8% to 62.6% with del32–71 GH induction, suggesting that the expression of del32–71 GH caused a dominant negative effect on wild-type GH secretion in these 20 cell lines (Figure 1A). Median wild-type GH concentrations among the 23 cell lines were 31.68 ng/mL (range, 7.78–84.00 ng/mL) and 18.18 ng/mL (range, 5.50–66.33 ng/mL), without and with del32–71 GH induction, respectively.

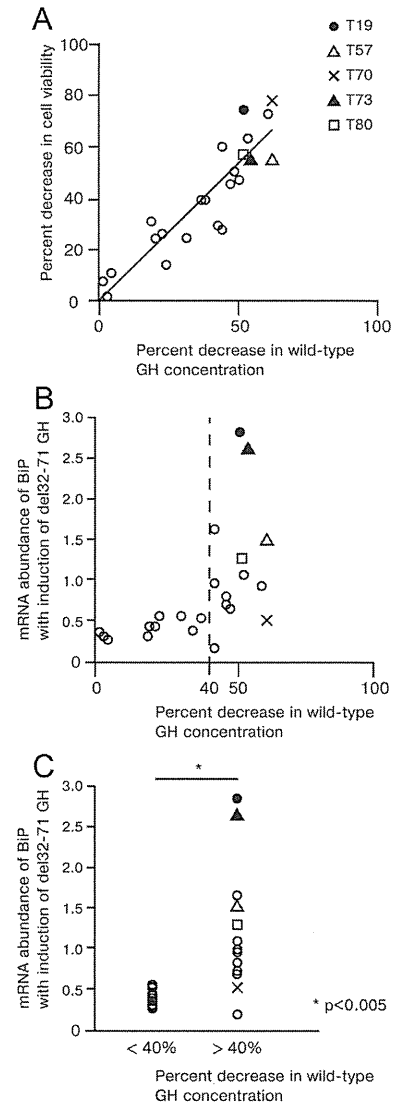

Figure 1. Demonstration of the dominant negative effect of del32–71 GH on wild-type GH secretion using cell lines with dox-controlled del32–71 GH expression. A and B, 23 cell lines with dox-controlled del32–71 GH expression were seeded at a density of 2.5×10^4 cells/150 μL in a 96-well culture plate in the presence or absence of 100 ng/mL dox. At 48 hours later, the concentrations of wild-type GH in the medium were measured by IRMA. Then, a 1/10 volume of CCK-8 reagent was added to the culture medium, and absorbance at 450 nm was measured 4 hours later using a multiplate reader. The relationships between the decrease in the wild-type GH concentration (−dox/+dox, horizontal axis) and the following factors (vertical axis) are shown: decrease in cell viability (−dox/+dox) (A) and mRNA abundance of BiP (−dox) by qRT-PCR normalized to β-actin (B). The dotted line indicates a 40% decrease in wild-type GH concentration. Each factor was measured 3 times, and means are shown. C, A difference in BiP transcripts between cells with decreases in wild-type GH secretion by less than 40% and cells with decreases by more than 40%. ●, T19 cell line; △, T57 cell line; ×, T70 cell line; ▲, T73 cell line; □, T80 cell line; ○, other dox-controlled cell lines.

Dominant negative effect was positively correlated with cell viabilities

Next, cell viabilities of the 23 dox-controlled cell lines were evaluated using CCK-8 reagent with or without induction. In the 20 clones in which the wild-type GH concentration in the culture medium decreased, cell viabilities also decreased by 14.3% to 78.0% after del32–71 GH induction. In addition, the wild-type GH concentrations in the culture medium were positively correlated with cell viability in these 23 cell lines, suggesting the association between the dominant negative effect of del32–71 GH and cell viability (Figure 1A).

mRNA abundance of ER stress markers was significantly higher in cells with large decreases in wild-type GH secretions than in cells with small decreases

The association between the dominant negative effect and cell viability led us to hypothesize that these 2 factors were associated with del32–71 GH–induced ER stress. To test this hypothesis, we evaluated a relationship between the wild-type GH concentrations (described above) and abundance of *BiP* transcripts with del32–71 GH induction in the 23 cell lines (Figure 1B). BiP was used as an ER stress marker because it is a well-known ER chaperone that binds to the hydrophobic region of unfolded proteins (see *Materials and Methods*) (12). A significant difference existed in *BiP* transcripts (normalized to β-actin) between cells with decreases in wild-type GH concentrations by less than 40% and those with decreases by more than 40% (Figure 1, B and C). Abundance of *XBP1(S)* transcripts, another ER stress response marker that enhances the transcription of ERAD components, was also evaluated with similar results (data not shown).

Five cell lines with dox-controlled del32–71 GH expression were selected as the cellular model

Thus, T19, T57, T70, T73, and T80 cell lines were chosen as the cellular model; wild-type GH secretion was severely decreased by the induction of del32–71 GH in these 5 cell lines, and the involvement of ER stress appeared to be large in T19 and T73 cells, medium in T57 and T80 cells, and small in T70 cells, as measured by *BiP* and *XBP1(S)* mRNA expression (Figure 1, A–C). We intentionally chose these 5 cell lines because *BiP* and *XBP1(S)* transcripts were variable even when wild-type GH secretion was decreased by more than 40% (Figure 1C).

qRT-PCR was performed to evaluate the expression of wild-type and del32–71 GH in these 5 cell lines. The expression of del32–71 GH increased 9.71- to 54.4-fold with the induction of del32–71 GH (Figure 2A), and, as a result, the abundance of del32–71 GH transcripts was compa-

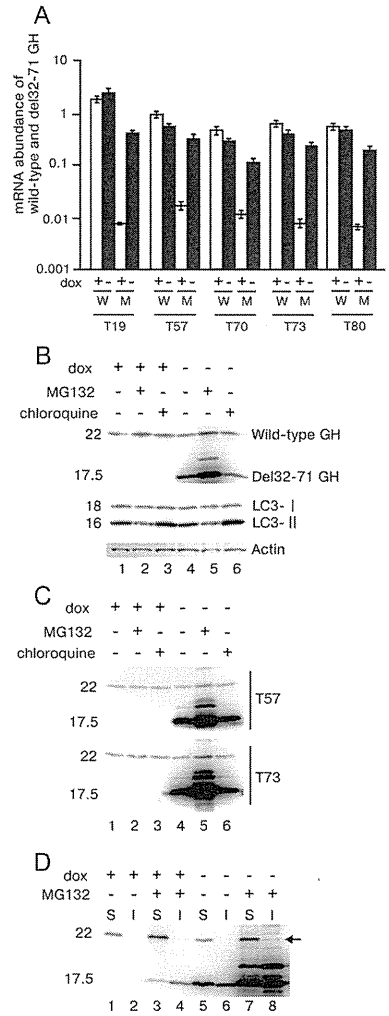

Figure 2. Evaluation of wild-type and del32–71 GH expression using the 5 cell lines with dox-controlled del32–71 GH expression. A, mRNA abundance of wild-type and del32–71 GH was evaluated by qRT-PCR using primers located within exon 3 for wild-type GH and spanning exon 2 and exon 4 for del32–71 GH; relative expression was calculated by normalization to β-actin expression. The means and SDs for 3 independent experiments were measured. W, wild-type GH; M, del32–71 GH. B, Immunoblotting of T19 cell lysate. Whole-cell lysates (30 μg/lane) were separated by SDS-PAGE, and immunoblotting was performed using antibodies for GH, LC3, and actin. Lane 1,100 ng/mL dox; lane 2, 10 μM MG132 with dox; lane 3, 50 μg/mL chloroquine with dox; lane 4, without dox; lane 5, 10 μM MG132 without dox; lane 6, 50 μg/mL chloroquine without dox. Similar results were obtained in 3 independent experiments. C, Immunoblotting of T57 and T73 cell lysates using antibodies for GH. Lane 1, 100 ng/mL dox; lane 2, 10 μM MG132 with dox; lane 3, 50 μg/mL chloroquine with dox; lane 4, without dox; lane 5, 10 μM MG132 without dox; lane 6, 50 μg/mL chloroquine without dox. D, Immunoblotting of soluble and insoluble fractions of T19 cell lysate using antibodies for GH. S, soluble fraction; I, insoluble fraction. Lanes 1 and 2, 100 ng/mL dox; lanes 3 and 4, 10 μM MG132 with dox; lanes 5 and 6, without dox; lanes 7 and 8, 10 μM MG132 without dox. Arrow indicates 22-kDa wild-type GH signal in insoluble fraction. The 17.5-kDa signals were detected even without the induction of del32–71 GH after MG132 treatment (lanes 3 and 4), indicating that leaky expression of del32–71 GH was observed.

rable with that of wild-type GH transcripts after the induction (Table 1). These data suggested that these 5 cell lines were appropriate cellular models for patients with the *GH1* gene splice site mutations; the transcript ratio of wild-type to del32–71 GH is theoretically 1:1.

del32–71 GH was degraded in a proteasome-dependent manner

Figure 2B shows the result of immunoblotting in T19 cell lysates. The removal of dox from the culture medium induced the expression of del32–71 GH, and treatment with the proteasome inhibitor MG132 markedly increased the 17.5-kDa signal, as reported previously (Figure 2B, lanes 4 and 5) (21, 22). The increase in the 17.5-kDa del32–71 GH signal was not demonstrated by chloroquine treatment, which disturbs lysosomal degradation by elevating the pH in the lysosome (Figure 2B, lanes 4–6). LC3-I is converted to LC3-II through the formation of autophagosomes, and LC3-II localizes in the autophagosomal membrane. Autophagosomes bind to lysosomes, and thus lysosomal inhibition is known to cause accumulation of LC3-II (23). Therefore, the increased LC3-II signal indicated that chloroquine treatment disturbed lysosomal function. These data suggested that del32–71 GH was a target of proteasome-dependent degradation, which is consistent with previous data demonstrating that del32–71 GH was localized within the ER (5, 6) and degraded via ERAD (21, 22). Note that MG132 is specific for ERAD. We confirmed the same pattern of immunoblotting in T57 and T73 cells (Figure 2C).

Coaggregation of wild-type and del32–71 GH was unlikely to be the major cause of the dominant negative effect

For the purpose of evaluating wild-type and del32–71 GH protein interactions, we investigated whether del32–71 GH coaggregated with wild-type GH. Unfolded proteins tend to aggregate, and such aggregated mutant proteins can involve normal proteins expressed from the other wild-type allele, causing a dominant negative effect (24). Previous studies have shown that aggregated mutant proteins have low solubility in 1% Triton X-100 (14, 22, 25). Thus, in the present study, T19 cells were lysed in 1% Triton X-100 in the presence or absence of del32–71 GH induction, and soluble/insoluble fractions were separately isolated for evaluation of each fraction by immunoblotting. A small amount (4.5%) of wild-type GH was detected in the insoluble fraction with the induction of del32–71 GH after MG132 treatment, whereas about half of del32–71 GH was detected in the insoluble fraction (Figure 2D, lanes 5–8). These data suggested that coaggregation of wild-type and del32–71 GH could exist but was unlikely to be the major cause of the dominant negative effect.

Table 1. mRNA Abundance Ratios for Wild-Type to del32–71 GH in the 5 dox-Controlled Cell Lines With and Without Induction of del32–71 GH

	mRNA Abundance Ratio of Wild-Type to del32–71 GH				
	T19	T57	T70	T73	T80
+ dox	229	51.4	39.0	79.6	85.8
− dox	5.74	1.71	2.60	1.69	2.33

Data represent ratios of the relative expression of wild-type to del32–71 GH (±100 ng/mL dox) evaluated by qRT-PCR after normalization to β-actin expression. Means of 3 independent experiments are shown.

del32–71 GH activated ER stress responses via the PERK, ATF6, and IRE1 pathways

The proteasome-dependent del32–71 GH degradation and the little involvement of wild-type GH in del32–71 GH aggregate led us to evaluate ER stress responses in the 5 cell lines with dox-controlled del32–71 GH expression. Three major pathways, the PERK, ATF6, and IRE1 pathways, are known to act as ER stress responses in mammalian cells as described in the Introduction. PERK, ATF6, and IRE1 are sensor molecules located in the membrane of the ER and are activated by the accumulation of unfolded proteins in the ER. These activated sensor molecules transduce signals to suppress the translation of proteins, enhance the folding capacity of ER chaperones, and promote the degrading function of ERAD machinery in the respective pathways (12). For each pathway, the following target genes were chosen: *GADD34* and *CHOP* for the PERK pathway, *BiP* and *GRP94* for the ATF6 pathway, and *XBP1* for the IRE1 pathway.

In T19, T57, T73, and T80 cell lines, the abundance of the target gene transcripts significantly increased after del32–71 GH induction, suggesting that the PERK and ATF6 pathways were activated by del32–71 GH induction in these 4 cell lines (Figure 3, A–D). In the T70 cell line, levels of these 4 target genes were significantly elevated, whereas the degree of activation was small compared with that of the other 4 cell lines (Figure 3, A–D).

In the same 4 cell lines, XBP1 was activated. XBP1 is a nuclear transcription factor that can be activated by IRE1, enhancing the transcription of ERAD components. IRE1 converts inactive *XBP1* [*XBP1(U)*] mRNA into active *XBP1* [*XBP1(S)*] mRNA by splicing out 26 bp, located between the DNA-binding domain and DNA-activating domain (12, 26, 27). The activation of *XBP1* can be detected by RT-PCR using primers that surround these 26 bp, yielding 140- and 114-bp PCR products corresponding to *XBP1(U)* and *XBP1(S)*, respectively. The higher the

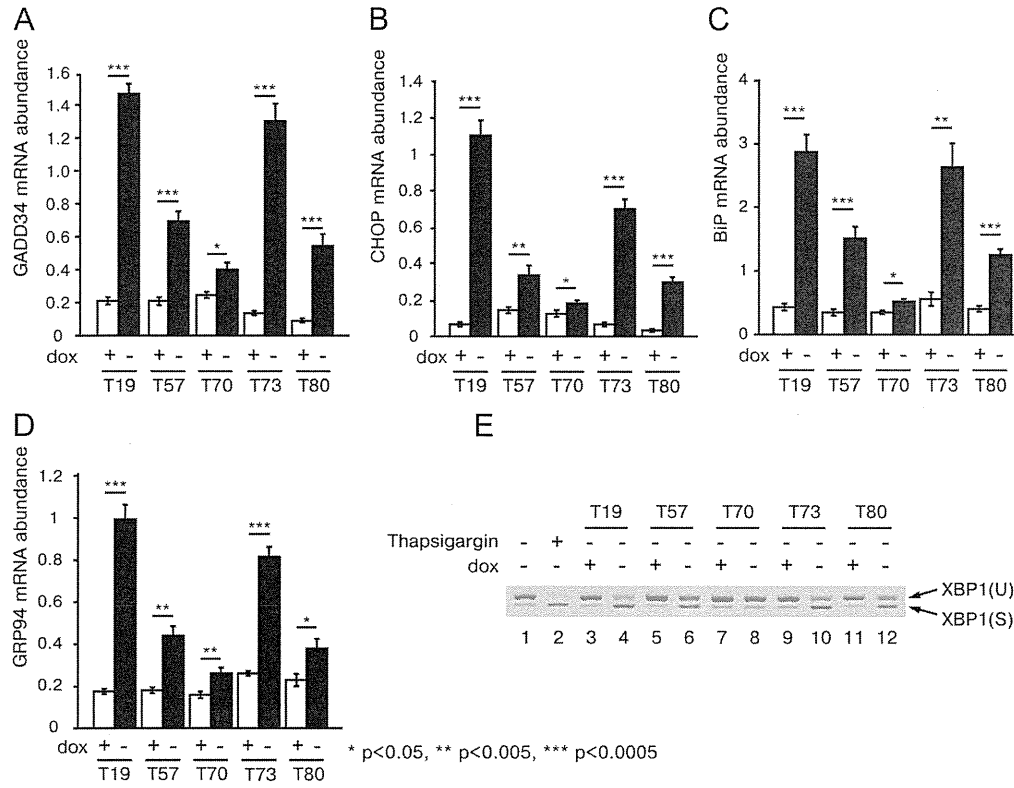

Figure 3. del32–71 GH induction activated ER stress responses via the PERK, ATF6, and IRE1 pathways. A–D, expression of GADD34 (A), CHOP (B), BiP (C), and GRP94 (D) transcripts in T19, T57, T70, T73, and T80 cell lines in the presence or absence of 100 ng/mL dox, as measured by qRT-PCR. Means and SDs from 3 independent experiments are shown, with relative abundance calculated by normalization to β-actin expression. Data were statistically evaluated using the Student *t* test. E, Splicing of XBP1 mRNA. mRNA from T19, T57, T70, T73, and T80 cell lines (±100 ng/mL dox) was converted to cDNA, and RT-PCR was performed. Samples were applied to a 3.5% agarose gel. XBP1(U), unspliced XBP1; XBP1(S), spliced XBP1; lane 1, untreated GH4C1 cells; lane 2, thapsigargin-treated GH4C1 cells; lanes 3 and 4, T19; lanes 5 and 6, T57; lanes 7 and 8, T70; lanes 9 and 10, T73; and lanes 11 and 12, T80. Similar results were obtained in 3 independent experiments for all 5 cell lines.

ratio of *XBP1(S)* to *XBP1(U)*, the more XBP1 is considered to be activated. As shown in Figure 3E, XBP1 was activated in T19, T57, T73, and T80 cell lines, suggesting that del32–71 GH induction activated the IRE1 pathway (Figure 3E, lanes 3–6 and 9–12). In the T70 cell line, XBP1 was not activated (Figure 3E, lanes 7 and 8).

In summary, all of the 3 major ER stress response pathways were demonstrated to be activated by the induction of del32–71 GH in T19, T57, T73, and T80 cell lines.

Dox treatment/removal could have some effects on cell physiology independent of del32–71 GH expression. Therefore, using the parental cell line expressing only wild-type GH, we evaluated wild-type GH concentrations in the media, cell viability, and ER stress responses. No significant differences were found after dox treatment/removal in this parental cell line, suggesting that dox administration itself did not have any significant effects on cell physiology (Supplemental Figure 1, A–D).

Marked proliferation and enlargement of the ER was observed by the induction of del32–71 GH under electron microscopy (EM)

To investigate the impact of del32–71 GH on cellular morphology, EM images of T80 cells were evaluated in the presence or absence of del32–71 GH induction. In high-power fields, marked proliferation and enlargement of the ER were demonstrated in some T80 cells after del32–71 GH induction (Figure 4, A–C). ER stress responses are known to stimulate ER synthesis to increase the folding capacity of ER chaperones, enhance the function of ERAD machinery, and dilute the unfolded protein load (28). Thus, these EM images were consistent with the activation of ER stress responses after del32–71 GH induction.

In low-power fields, many vacuoles appeared within the cytosol after the induction of del32–71 GH expression (Figure 4D). The number of vacuoles varied in T80 cells, ie, vacuoles did not exist in all induced T80 cells. However, ratios of vacuole area to cytosol area were significantly increased after induction (Figure 4E). Although autophagy is another mechanism through which unfolded

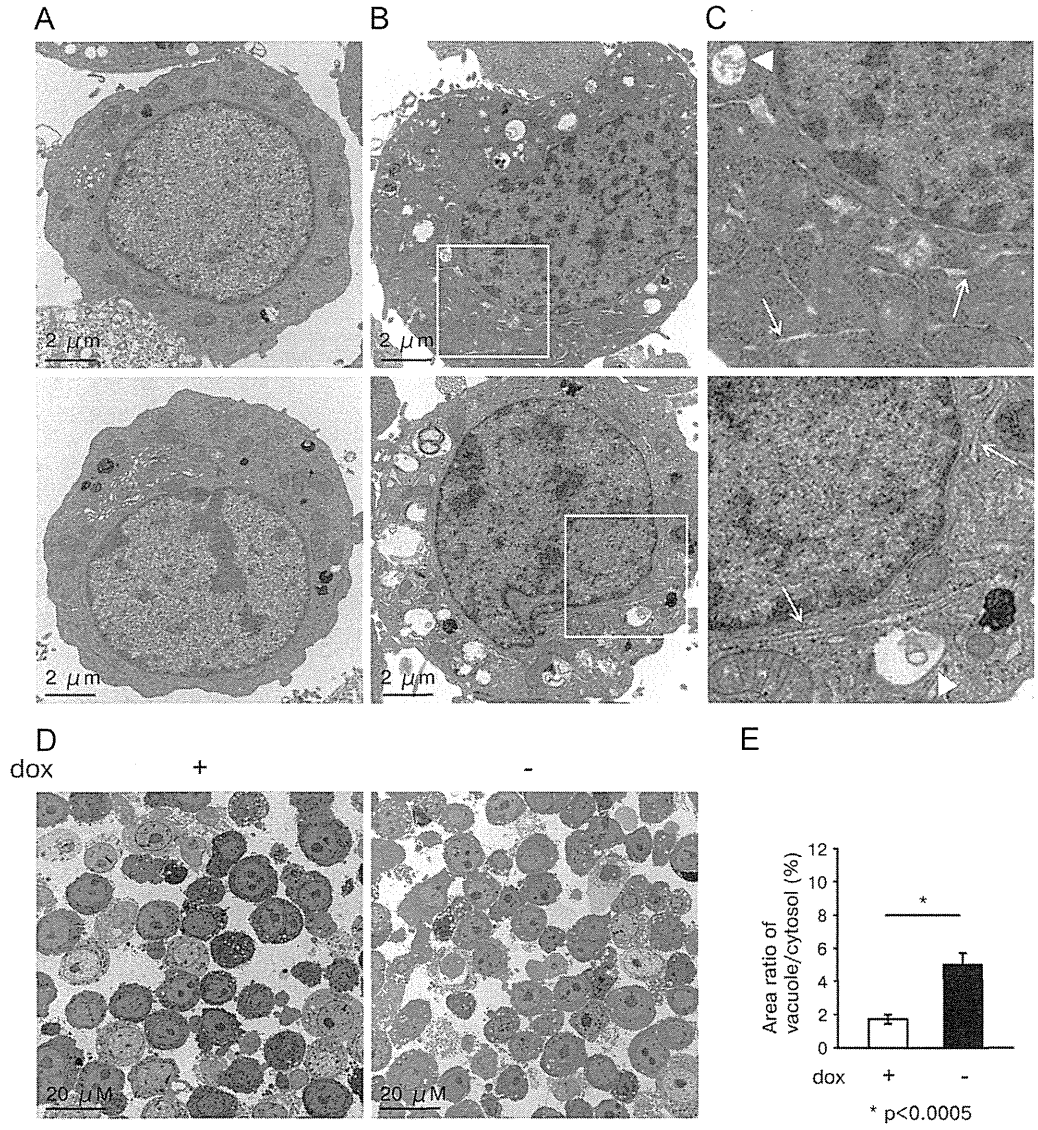

Figure 4. EM images of the T80 cell line. A, High-power fields, in the presence of 100 ng/mL dox. B, High-power fields, in the absence of dox. C, Enlarged pictures of the indicated areas in B. Marked accumulation of the rough ER (arrow) and vacuoles (arrowhead) was observed. D, Low-power fields, in the presence or absence of dox. The number of vacuoles was increased by del32–71 GH induction. E, Ratio of vacuole area to cytosol area was calculated using WinROOF. Means and SEMs for 29 and 36 EM images, without and with del32–71 GH induction, respectively, were statistically evaluated by the Student *t* test.

protein can be degraded and is known to be activated by ER stress (23), these vacuoles were not thought to be LC3-dependent autophagosomes; LC3-II translocation was not shown by either immunoblotting (Figure 2B, lanes 1 and 4) or immunofluorescence (data not shown).

Induction of del32–71 GH caused apoptosis

Next, we evaluated whether the induction of del32–71 GH caused apoptosis in these cells. DNA samples from T19 cells were extracted every 12 hours after del32–71 GH induction and subjected to electrophoresis. Induction of del32–71 GH for 12 hours caused DNA fragmentation in T19 cells, suggesting the occurrence of apoptosis (Figure 5A).

del32–71 GH induction also caused activation of caspase-3 and -7, an early sign of apoptosis, in T19, T57, T73, and T80 cells (Figure 5, B and C). Caspases are well-known proapoptotic components, and caspase-3 and -7 have been reported to be involved in ER stress–induced cell death (29). With use of the image-analyzing software WinROOF, caspase-positive (apoptotic) cells and Hoechst33428-positive (surviving) cells were counted (see *Materials and Methods*). Ratios of caspase-positive cells to total cells were significantly increased with the induction

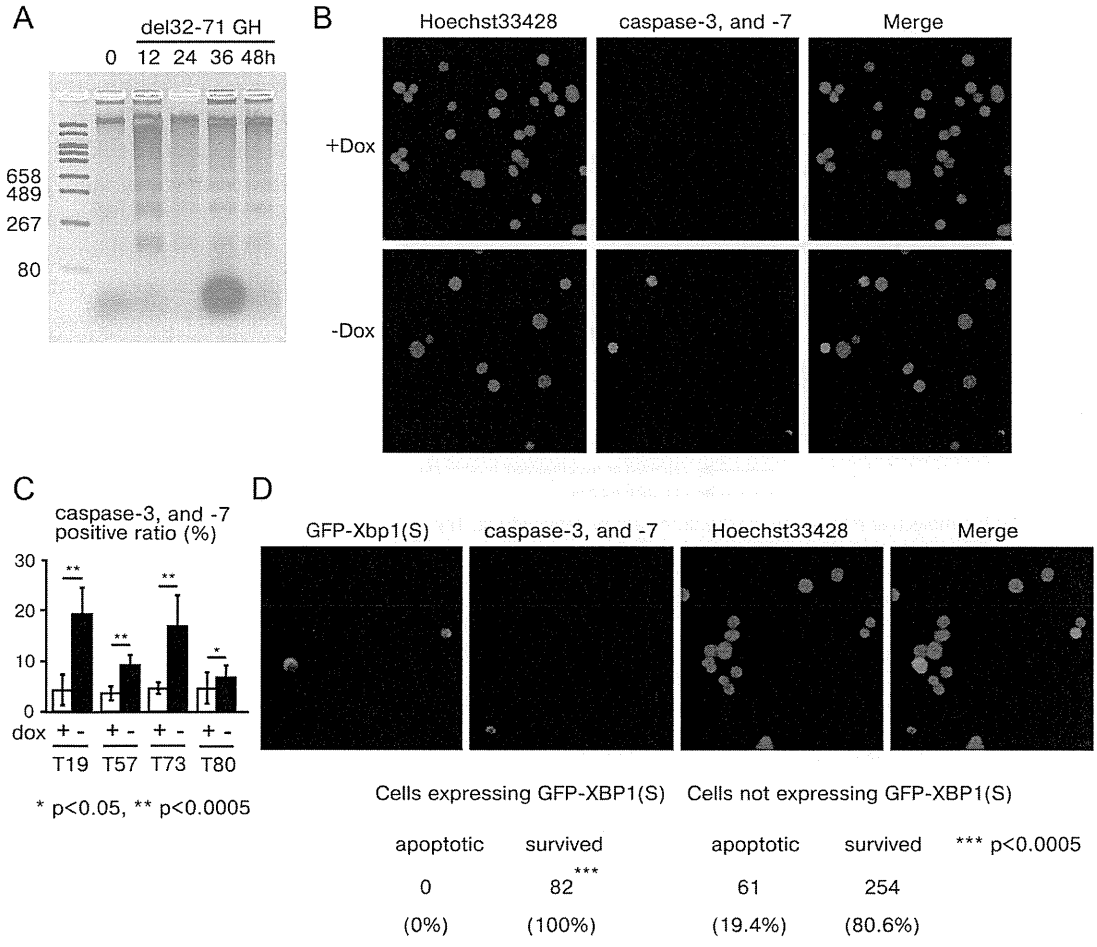

Figure 5. del32–71 GH induction caused ER stress, leading to apoptosis. A, DNA fragmentation caused by the induction of del32–71 GH. T19 cells were incubated without dox for the indicated times and evaluated for DNA fragmentation. Chromosomal DNA was extracted, separated on a 2% agarose gel and then visualized by staining with GelRed. B, Activation of caspase-3 and -7 by the induction of del32–71 GH. The expression of del32–71 GH was induced in T19, T57, T73, and T80 cell lines, and the activation of caspase-3 and -7 was evaluated 24 hours later using the Image-iT LIVE Red Caspase-3 and -7 Detection Kit. Hoechst33428-positive cells indicate surviving cells, and rhodamine-positive cells indicate apoptotic cells. C, The ratio of rhodamine-positive cells to total cells in B was calculated by WinROOF. Means and SDs for 10 independent experiments were measured, and statistical evaluations were conducted using the Student *t* test. D, GFP-XBP1(S) was overexpressed in T73 cells, and the expression of del32–71 GH was induced 24 hours later. After an additional 24 hours, activation of caspase-3 and caspase-7 was evaluated, and cells were photographed under a fluorescence microscope. The numbers of apoptotic and surviving cells were counted (bottom). The data were statistically evaluated using the χ^2 test.

of del32–71 GH in these 4 cell lines, suggesting that del32–71 GH–induced apoptosis was associated with ER stress (Figure 5C).

Overexpression of XBP1(S) rescued del32–71 GH–mediated apoptosis

To confirm a causal relationship between ER stress and apoptosis, we finally examined whether the introduction of XBP1(S), a nuclear transcription factor that enhances the transcription of ERAD components, could rescue del32–71 GH–induced apoptosis. In a previous study, overexpression of XBP1(S) was reported to rescue thapsigargin-induced apoptosis (27). Thus, T73 cells were transfected with GFP-XBP1(S) followed by induction of del32–71 GH expression and evaluation for the activation of caspase-3 or -7. The overexpression of XBP1(S) completely reversed the activation of caspase-3 and -7 (Figure 5D), suggesting that the induction of del32–71 GH caused ER stress, which subsequently triggered apoptosis.

Discussion

Our hypothesis for the molecular mechanism of the dominant negative effect, together with data reported in other studies, is shown in Figure 6. The major finding of our study was that the induction of del32–71 GH activated ER stress responses, causing apoptosis in our pituitary-derived cell lines.

Several studies have investigated the molecular mechanisms mediating the dominant negative effect of

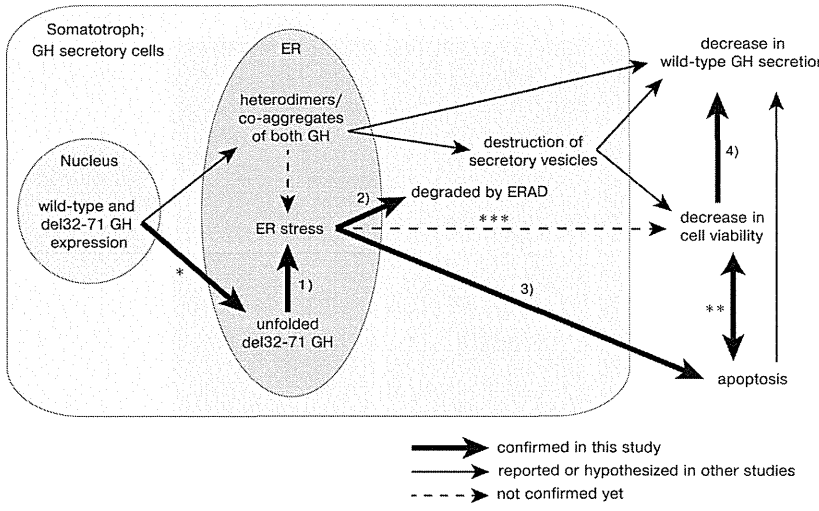

Figure 6. A model for the molecular mechanism of the dominant negative effect. Thick arrows represent data confirmed in the current study, arrows represent data reported in other studies, and dashed arrows represent data not confirmed yet. In this study, we demonstrated that (1) ER-localized del32–71 GH caused ER stress, (2) del32–71 GH was degraded by a proteasome-dependent manner via ERAD, (3) ER stress caused by del32–71 GH triggered apoptosis, and (4) the decrease in cell viability and wild-type GH secretion were associated. *, We confirmed localization of del32–71 GH in the ER by an immunofluorescence study (data not shown). **, It is difficult to evaluate a causal association between the decrease in cell viability and apoptosis; the former can be a result of the latter and vice versa. ***, A causal relationship between ER stress and decrease in cell viability is speculated but not proven; we did not evaluate cell viability and wild-type GH secretion in the cells that are rescued by overexpression of XBP1(S).

del32–71 GH. Hayashi et al (30) showed that cotransfection of wild-type and del32–71 GH leads to a decrease in wild-type GH secretion using pituitary-derived cell lines. Iliev et al (31), Lee et al (32), and Salemi et al (33) demonstrated that transfection of neuroendocrine cells with wild-type GH and del32–71 GH suppresses the accumulation and secretion of wild-type GH. McGuinness et al (7) demonstrated a decrease in the proliferation rate and destruction of secretory vesicles using GC cells stably expressing del32–71 GH, and Kannenberg et al (22) established double-transfected stable GH4C1 cell lines using wild-type and del32–71 GH constructs, demonstrating that aggregated wild-type and del32–71 GH were degraded by the proteasome. These previously published data suggested that the dominant negative effect of del32–71 GH may be caused by protein interactions, such as coaggregates of wild-type and del32–71 GH.

Theoretically, del32–71 GH exerts a dominant negative effect on the production and secretion of wild-type GH in 3 steps: (1) mRNA levels, reducing wild-type GH mRNA by mechanisms such as rapid degradation; (2) protein levels, promoting degradation of wild-type GH with degradation of del32–71 GH as a result of heterodimers or aggregates; and (3) cellular characteristics, including a decrease in overall cell viability and apoptosis, for example, that caused by ER stress. In our study, involvement of the first step in the dominant negative effect was unlikely because the abundance of wild-type GH transcripts did not change with del32–71 GH induction (Figure 2A). Hamid et al (34) reported that both the amount of del32–71 or wild-type GH transcripts and the ratio of del32–71 to wild-type GH transcripts correlated with differences in height SD scores in patients with the same *GH1* gene splice site mutation (34). These data suggested that some unknown function of del32–71 GH, which acts to suppress the transcription or promote the degradation of wild-type GH mRNA, may exist.

Next, we speculated that the involvement of the second step, protein interactions, in the dominant negative effect was unlikely, because little wild-type GH was detected in the insoluble fraction with the induction of del32–71 GH after MG132 treatment (Figure 2D). However, previous reports have demonstrated that wild-type and del32–71 GH coaggregate (7, 22). Heterodimers and the involvement of wild-type GH in del32–71 GH aggregates are both widely accepted as the most likely explanations for the mechanism of the coaggregation. McGuinness et al (7) hypothesized that heterodimers, which block the formation of dense-cored secretory vesicles, overwhelming the capacity of degradation, can destroy secretory vesicles, leading to aggregation within the cytosol. If this hypothesis is true, wild-type and del32–71 GH should colocalize in secretory vesicles. However, to date, no studies have demonstrated definitive evidence of heterodimers or their colocalization in secretory vesicles. Thus, more detailed evaluations of the interactions between wild-type and del32–71 GH and their subcellular localization are needed.

The third step, a decrease in cell viability, appeared to play a pivotal role in the dominant negative effect in our study. Using GH4C1 cell lines with dox-controlled del32–71 GH expression, we demonstrated that the induction of del32–71 GH decreased wild-type GH secretion and cell viability. The positive correlation between wild-type GH secretion and cell viability suggested that del32–71 GH had a toxic effect on cell physiology. qRT-PCR revealed activation of the 3 major ER stress response pathways, and EM images showed proliferation and enlargement of the ER. The del32–71 GH induction caused DNA fragmentation and activation of caspase-3 and -7, early signs of apoptosis. Finally, overexpression of

XBP1(S) completely reversed the activation of caspase-3 and -7, confirming the causal relationship between del32–71 GH–induced ER stress and apoptosis. Salemi et al (33) demonstrated that del32–71 GH caused reductions in cell proliferation, DNA fragmentation, and apoptosis using fluorescence-activated cell sorting analysis in AtT-20 cell lines. Our data indicate that the effect reported by Salemi et al (33) can be at least partially explained by del32–71 GH–induced ER stress. However, it is still not clear from our study whether ER stress was caused by del32–71 GH alone or by both wild-type and del32–71 GH.

We cannot conclude that ER stress is the sole cause of the dominant negative effect because the T70 cell line demonstrated minimally activated ER stress responses despite the decrease in cell viability and wild-type GH secretion after del32–71 GH induction. Thus, mechanisms other than ER stress must be involved in the dominant negative effect observed in the T70 cell line. However, the involvement of ER stress was definite in the other 4 cell lines in the current study, and thus we consider ER stress to be one of the factors contributing to the dominant negative effect. Our data may complement previous hypotheses such as destruction of secretory vesicles or degradation of aggregated wild-type and del32–71GH.

In our study, the influence of the GHRH signal on the transcription of wild-type and del32–71 GH was not taken into account. Salemi et al (33) and Petkovic et al (21) reported that GHRH stimulation increases del32–71 GH expression preferentially and causes GH deficiency in a vicious cycle. We also note that patients with the *GH1* gene splice site mutations have variable phenotypes, depending on the site of the intronic mutation. The expression of del32–71 GH was shown to increase corresponding with increasing proximity of mutations to the IVS3 splice site (33). We are not able to highlight these various effects because of the use of cDNA constructs. Therefore, we expect that the in vivo dominant negative effect would be much more complex.

Thus, evaluating somatotrophs in vivo using mouse models will give us clues to more thoroughly elucidate the molecular mechanisms mediating the dominant negative effect of del32–71 GH. McGuinness et al (7) established a human del32–71 GH transgenic mouse model and observed severe cellular damage to pituitary cells in this model. Mouse models in which the human wild-type *GH1* gene and human del32–71 *GH1* gene are knocked-in (replacing the mouse *gh1* gene) may be powerful tools in the evaluation of this dominant negative effect and may facilitate the development of new therapeutic interventions, such as overexpression of XBP1(S).

In conclusion, ER stress and apoptosis play a significant role in the dominant negative effect of del32–71 GH resulting from the *GH1* gene splice site mutations. This may explain the evolution of GH deficiency in this disorder. More detailed in vivo studies are necessary in the future.

Acknowledgments

We thank Kazue Kinoshita for assistance with maintenance of cells, Toshimi Michigami for teaching us how to establish stably transfected cell lines, Masahiro Kaburagi for help with measuring wild-type GH concentrations in the culture media by IRMA, Wataru Takahashi and Ryuji Fukuzawa for help with taking EM images, Yasuo Uchiyama and Masaaki Komatsu for advice on the detection of LC3-dependent autophagy activation, Kimi Araki and Ken-ichi Yamamura for providing us antibodies for immunofluorescence studies, and Pinchas Cohen for proofreading of the manuscript.

Address all correspondence and requests for reprints to: Yukihiro Hasegawa, Department of Endocrinology, Tokyo Metropolitan Children's Medical Center, 2–8-29, Musashidai, Fuchu, Tokyo 183–8561, Japan. E-mail: yukihiro_hasegawa@tmhp.jp.

This study was supported by grants from Tokyo Metropolitan Foundation (to Y.H.) and the Foundation of Growth Science in Japan (to D.A.).

Disclosure Summary: The authors have nothing to disclose.

References

1. **Binder G, Ranke MB.** Screening for growth hormone (GH) gene splice-site mutations in sporadic cases with severe isolated GH deficiency using ectopic transcript analysis. *J Clin Endocrinol Metab.* 1995;80:1247–1252.
2. **Cogan JD, Phillips JA, 3rd, Schenkman SS, Milner RD, Sakati N.** Familial growth hormone deficiency: a model of dominant and recessive mutations affecting a monomeric protein. *J Clin Endocrinol Metab.* 1994;79:1261–1265.
3. **Akinci A, Kanaka C, Eble A, Akar N, Vidinlisan S, Mullis PE.** Isolated growth hormone (GH) deficiency type IA associated with a 45-kilobase gene deletion within the human GH gene cluster. *J Clin Endocrinol Metab.* 1992;75:437–441.
4. **Ultsch MH, Somers W, Kossiakoff AA, de Vos AM.** The crystal structure of affinity-matured human growth hormone at 2 A resolution. *J Mol Biol.* 1994;236:286–299.
5. **Graves TK, Patel S, Dannies PS, Hinkle PM.** Misfolded growth hormone causes fragmentation of the Golgi apparatus and disrupts endoplasmic reticulum-to-Golgi traffic. *J Cell Sci.* 2001;114:3685–3694.
6. **Salemi S, Yousefi S, Eble A, Deladoey J, Mullis PE.** Impact of del32–71-GH (exon 3 skipped GH) on intracellular GH distribution, secretion and cell viability: a quantitative confocal microscopy analysis. *Horm Res.* 2006;65:132–141.
7. **McGuinness L, Magoulas C, Sesay AK, et al.** Autosomal dominant growth hormone deficiency disrupts secretory vesicles in vitro and in vivo in transgenic mice. *Endocrinology.* 2003;144:720–731.
8. **Harding HP, Zhang Y, Ron D.** Protein translation and folding are coupled by an endoplasmic-reticulum-resident kinase. *Nature.* 1999;397:271–274.
9. **Haze K, Yoshida H, Yanagi H, Yura T, Mori K.** Mammalian transcription factor ATF6 is synthesized as a transmembrane protein and

activated by proteolysis in response to endoplasmic reticulum stress. *Mol Biol Cell.* 1999;10:3787–3799.
10. **Yoshida H, Haze K, Yanagi H, Yura T, Mori K.** Identification of the cis-acting endoplasmic reticulum stress response element responsible for transcriptional induction of mammalian glucose-regulated proteins: involvement of basic leucine zipper transcription factors. *J Biol Chem.* 1998;273:33741–33749.
11. **Tirasophon W, Welihinda AA, Kaufman RJ.** A stress response pathway from the endoplasmic reticulum to the nucleus requires a novel bifunctional protein kinase/endoribonuclease (Ire1p) in mammalian cells. *Genes Dev.* 1998;12:1812–1824.
12. **Yoshida H.** ER stress and diseases. *FEBS J.* 2007;274:630–658.
13. **Fonseca SG, Fukuma M, Lipson KL, et al.** WFS1 is a novel component of the unfolded protein response and maintains homeostasis of the endoplasmic reticulum in pancreatic beta-cells. *J Biol Chem.* 2005;280:39609–39615.
14. **Imai Y, Soda M, Inoue H, Hattori N, Mizuno Y, Takahashi R.** An unfolded putative transmembrane polypeptide, which can lead to endoplasmic reticulum stress, is a substrate of Parkin. *Cell.* 2001; 105:891–902.
15. **Ito M, Jameson JL, Ito M.** Molecular basis of autosomal dominant neurohypophyseal diabetes insipidus. Cellular toxicity caused by the accumulation of mutant vasopressin precursors within the endoplasmic reticulum. *J Clin Invest.* 1997;99:1897–1905.
16. **Katayama T, Imaizumi K, Honda A, et al.** Disturbed activation of endoplasmic reticulum stress transducers by familial Alzheimer's disease-linked presenilin-1 mutations. *J Biol Chem.* 2001;276: 43446–43454.
17. **Olias G, Richter D, Schmale H.** Heterologous expression of human vasopressin-neurophysin precursors in a pituitary cell line: defective transport of a mutant protein from patients with familial diabetes insipidus. *DNA Cell Biol.* 1996;15:929–935.
18. **Oyadomari S, Koizumi A, Takeda K, et al.** Targeted disruption of the Chop gene delays endoplasmic reticulum stress-mediated diabetes. *J Clin Invest.* 2002;109:525–532.
19. **Sambrook J, Eritsch E, Maniatis T.** *Molecular Cloning: A Laboratory Manual.* New York, NY: Cold Spring Harbor Laboratory Press.
20. **Ishiyama M, Miyazono Y, Sasamoto K, Ohkura Y, Ueno K.** A highly water-soluble disulfonated tetrazolium salt as a chromogenic indicator for NADH as well as cell viability. *Talanta.* 1997;44:1299–1305.
21. **Petkovic V, Godi M, Lochmatter D, et al.** Growth hormone (GH)-releasing hormone increases the expression of the dominant-negative GH isoform in cases of isolated GH deficiency due to GH splice-site mutations. *Endocrinology.* 2010;151:2650–2658.
22. **Kannenberg K, Wittekindt NE, Tippmann S, Wolburg H, Ranke MB, Binder G.** Mutant and misfolded human growth hormone is rapidly degraded through the proteasomal degradation pathway in a cellular model for isolated growth hormone deficiency type II. *J Neuroendocrinol.* 2007;19:882–890.
23. **Ogata M, Hino S, Saito A, et al.** Autophagy is activated for cell survival after endoplasmic reticulum stress. *Mol Cell Biol.* 2006;26: 9220–9231.
24. **Albrecht AN, Kornak U, Boddrich A, et al.** A molecular pathogenesis for transcription factor associated poly-alanine tract expansions. *Hum Mol Genet.* 2004;13:2351–2359.
25. **Ward CL, Omura S, Kopito RR.** Degradation of CFTR by the ubiquitin-proteasome pathway. *Cell.* 1995;83:121–127.
26. **Yoshida H, Matsui T, Yamamoto A, Okada T, Mori K.** XBP1 mRNA is induced by ATF6 and spliced by IRE1 in response to ER stress to produce a highly active transcription factor. *Cell.* 2001; 107:881–891.
27. **Yoshida H, Nadanaka S, Sato R, Mori K.** XBP1 is critical to protect cells from endoplasmic reticulum stress: evidence from site-2 protease-deficient Chinese hamster ovary cells. *Cell Struct Funct.* 2006; 31:117–125.
28. **Schroder M, Kaufman RJ.** Divergent roles of IRE1α and PERK in the unfolded protein response. *Curr Mol Med.* 2006;6:5–36.
29. **Dahmer MK.** Caspases-2, -3, and -7 are involved in thapsigargin-induced apoptosis of SH-SY5Y neuroblastoma cells. *J Neurosci Res.* 2005;80:576–583.
30. **Hayashi Y, Yamamoto M, Ohmori S, Kamijo T, Ogawa M, Seo H.** Inhibition of growth hormone (GH) secretion by a mutant GH-I gene product in neuroendocrine cells containing secretory granules: an implication for isolated GH deficiency inherited in an autosomal dominant manner. *J Clin Endocrinol Metab.* 1999;84:2134–2139.
31. **Iliev DI, Wittekindt NE, Ranke MB, Binder G.** Structural analysis of human growth hormone with respect to the dominant expression of growth hormone (GH) mutations in isolated GH deficiency type II. *Endocrinology.* 2005;146:1411–1417.
32. **Lee MS, Wajnrajch MP, Kim SS, et al.** Autosomal dominant growth hormone (GH) deficiency type II: the Del32–71-GH deletion mutant suppresses secretion of wild-type GH. *Endocrinology.* 2000;141: 883–890.
33. **Salemi S, Yousefi S, Lochmatter D, et al.** Isolated autosomal dominant growth hormone deficiency: stimulating mutant GH-1 gene expression drives GH-1 splice-site selection, cell proliferation, and apoptosis. *Endocrinology.* 2007;148:45–53.
34. **Hamid R, Phillips JA 3rd, Holladay C, et al.** A molecular basis for variation in clinical severity of isolated growth hormone deficiency type II. *J Clin Endocrinol Metab.* 2009;94:4728–4734.

特　集　最近話題のホルモン受容体異常症

GHRH受容体異常症

曾根田 明子*　安達 昌功*

1 疾患概念

下垂体前葉からの成長ホルモン(GH)分泌は，主として視床下部のGH放出ホルモン(GHRH)およびソマトスタチンにより制御されている．GHRH受容体異常症とは，下垂体ソマトトロフに発現するGHRH受容体の先天的異常のため生じるGH単独欠損症(isolated Growth Hormone deficiency : IGHD)をいう．

IGHDは，出生後に始まる成長障害を主徴とし，その頻度は4,000～10,000出生に1人と報告されている[1-3]．このうちの多くは特発性であり，また一部は視床下部～下垂体領域における虚血・炎症・腫瘍等の後天的要因によるものである．遺伝子異常による遺伝性IGHDは稀であり，報告により5～30％とされている[4]．

遺伝性IGHDは臨床的特徴や遺伝形式等により4つのタイプに分類されている(表1)．GHRH受容体異常症はタイプIBに分類され，常染色体劣性の遺伝形式を呈する．

2 GHRH受容体

GHRH受容体はG蛋白共役受容体(G-protein coupling receptor : GPCR)の一つであり，423のアミノ酸より構成されている．GPCRファミリーの中のBグループIIIに属し，細胞外N末端領域，7回膜貫通領域，および細胞内C末端領域を有する．リガンドであるGHRHが受容体に結合することで，セカンドメッセンジャーであるcAMPの合成が促され，プロテインキナーゼA経路の活性化を経てGHが分泌される．また，リガンドの結合によるMAPキナーゼ活性化も報告されている[5,6]．GHRH受容体遺伝子(*GHRHR*)は常染色体7p14に存在し，13個のエクソンより成り立っている[7]．

3 GHRH受容体遺伝子(*GHRHR*)変異の報告例

最初のGHRH受容体遺伝子異常として，1993年に遺伝性GH欠損マウスモデルであるLittleマウスにおけるホモ接合体変異(D60G)が見いだされた[8,9]．

ヒトでは，1990年代後半に2つの変異が低身長の大家系で発見されている．1つは，インド[10]，パキスタン[11]，スリランカ[12]から報告されたエクソン3のE72X変異であり，後にこれらはリンケージ解析で共通の祖先に由来することが判明した[13]．他方は，ブラジル北東部の大家族例から報告された，スプライス変異(IVS1+1g>a)である[14]．

現在までに，プロモーター領域の変異，ミスセンス変異，ナンセンス変異，スプライス異常，微小欠失を合わせ，約20の*GHRHR*変異が報告されている(表2)．多くは前述のように一定の地域に限局した血族婚のある家系からの報告であり，孤

* 神奈川県立こども医療センター　内分泌代謝科
Akiko Soneda : GHRH receptor mutation.
Department of Endocrinology & Metabolism, Kanagawa Children's Medical Center.

表1　遺伝性IGHDの分類

タイプ	遺伝形式	原因遺伝子	GH分泌	特徴
I A	AR	*GH1* 欠失/*GH1* 変異	欠損	重度の低身長．治療による抗GH抗体が出現が見られる
I B	AR	*GH1* 変異/*GHRHR* 変異	低下	低身長．GH治療に対する反応は良好
II	AD	*GH1* 変異	低下	低身長．GH治療に対する反応は良好
III	X連鎖	*BTK* 変異/未同定	低下	*BTK* 変異は低ガンマグロブリン血症を伴う

AD：常染色体優性，AR：常染色体劣性

表2　既報のGHRH受容体異常症のまとめ

変異	国・地域名	性別	報告時の年齢	身長SDS	負荷試験でのGH頂値 (ng/mL) GHRH	インスリン	IGF-1 (ng/mL)	下垂体低形成 (検査時年齢)
-124A>C / K329F	不明	M	4y	-4.6	1.6	1.2		+(4y)
IVS1+1G>A ホモ	ブラジル	M9, F13	5y ~ 20y	-2.7 ~ -8.4	0.63 ± 0.61	"flat"	6.7 ± 2.8	ND
IVS1+1G>A / IVS4-2A>G	ブラジル	F	9y	-6.2		1.5		+(9y)
IVS1+1G>A / E382E	ブラジル	F	7y	-3.3		0.1		+(16y)
IVS1+2T>G ホモ	モロッコ	M1, F1	9y, 11y	-5.4 ~ -6.6		0.1 ~ 4.2	17.4 ~ 21	+(9y), +(14y)
Q43X / IVS3+1G>A	不明	M2	8y, 11y	-5.5	<0.05		16 ~ 20	+(18y), +(20y)
IVS2+3A>G / G136V	日本	F	2y	-3.1	3.93	2.81	7	-(2y)
E72X ホモ	多数報告例あり							
E72X　R161W	アジア	M1, F1	4y, 5y	-4.5 ~ -4.8		0.6 ~ 0.7	<-2.5SD	-(4y), +(5y)
R94L ホモ	アジア	F	5y	-5.6		0.9	-3.0SD	+(5y)
391delG ホモ	エジプト	F3	5.9y	-5.5 ~ -6.0			<6 ~ 9	-(4y), +(5y)
H137L / del 1140-1144	不明	M1, F1	11y, 14y	-5.9 ~ -7.0		1.0		ND
L144H ホモ	スペイン	M2	3y ~ 5y	-3.3 ~ -4.0	0.41 ~ 2.0		22 ~ 30	+(5y)
	ブラジル	F2	19y ~ 26y	-7.1 ~ -7.4	<0.3	<0.3	2.5 ~ 4.6	+(19y), +(26y)
L144H / F242C	米国	M2	16y ~ 17y	-4.5 ~ -5.2		2.3 ~ 3.8		ND
A176V ホモ	パキスタン	M2	8y	-3.5 ~ -4.5	<1mU/L			+(8y)
A222E ホモ	パキスタン	M2	2y ~ 11y	-5.2 ~ -6.8				ND
	アジア	M1, F1	2y, 3y	-2.8 ~ -3.0		0.4	<-3.5SD	-+(3y)
IVS7+1G>C ホモ	モロッコ	M1, F1	14y, 16y	-5.1 ~ -7.3	"absent"		14.5 ~ 26.8	-(23y), -(25y)
IVS7-1G>A ホモ	ブラジル	M1, F1	3y ~ 10y	-2.5 ~ -3.9	1.8 ~ 2.6		18	ND
IVS8+1G>A ホモ	中国	F3	36y ~ 56y	120 ~ 121cm		0.15	31.5	+(36y), +(42y)
W273S ホモ	アジア	F2	2y ~ 6y	-2.8 ~ -4.9		0.9	-1.9SD ~ -3.5SD	-(2y), +(6y)
E382E ホモ	日本	F2	5y, 7y	-5.2 ~ -5.6	2.0			-(5y), -(7y)
del 1121-1124 ホモ	日本	M	3y	-6.0	0.2		67.9	+(3y)
IVS12+2T>A ホモ	パキスタン	M1, F2	2y ~ 8y	-2.5 ~ -3.6	0.6 ~ 1.0		11, 49	+(3y), -(3y), -(8y)

文献19より一部改編
M 男性，F 女性．ND not done.

発例の報告は少ない．IGHDを呈し，正常位置に下垂体が観察された224名の遺伝子解析を行ったイギリスの報告では，7家系・15例に*GHRHR*変異が発見されたが，いずれもnon-Caucasianで，両親の血族婚を有する家族からの症例であった[15]．また，IGHD患者89名を対象にしたオランダからの報告では*GHRHR*変異は同定されなかった[16]．

国内では4例のGHRH受容体異常症が報告され

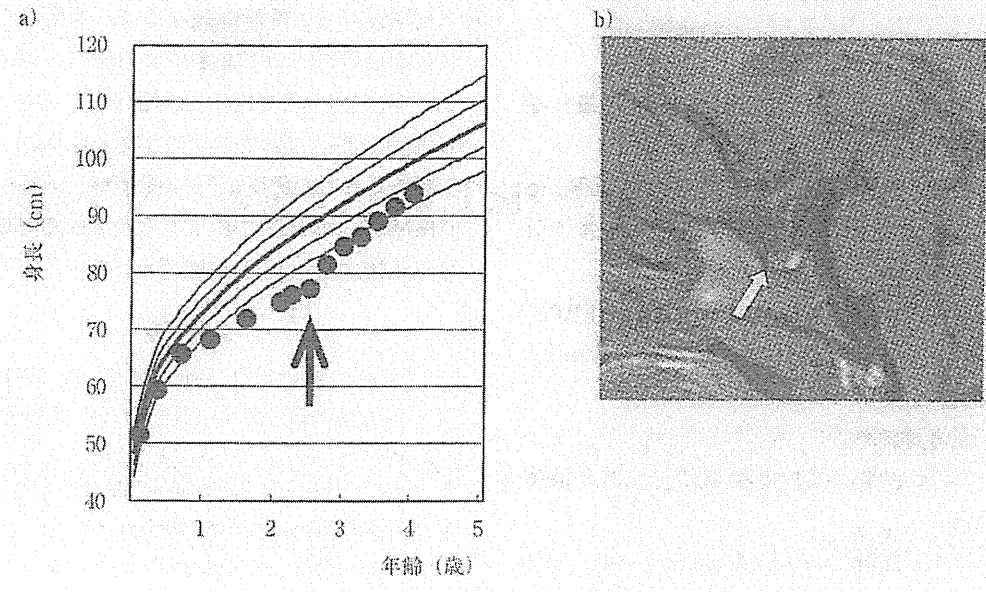

図1 a) 成長曲線．矢印はGH補充療法開始時を示す．
b) 下垂体MRI画像．

ている．堀川によるエクソン12の4塩基欠失例（del1121-1124）[17]，井上らによるE382Eの同胞例[18]，筆者らによるG136VとIVS2+3a>gとの複合ヘテロ接合体変異（後述）であり[19]，これらはいずれも血族婚を有さない症例である．井上らの検討では，IGHD 14例および特発性低身長113例においてGHRHR解析が行われたが，E382E同胞例以外には変異は見いだされなかった[18]．

4 臨床症状

全例が重篤な低身長を呈する．子宮内での発育障害は見られず，成長障害は1歳前後から観察される．無治療の症例では-4～-8SDの低身長となる．知能発達は正常であり，GH-1遺伝子異常症で観察される新生児低血糖は見られず，また前額部突出や腹部肥満はあっても軽度である[20]．男児では小陰茎は認めない．

血液検査所見ではIGF-1が低値を示す．GH分泌刺激試験に対するGH分泌も不良であり，多くの症例は重症成長ホルモン分泌不全性低身長症の所見を示す．他の下垂体ホルモン分泌に異常は見られない．一部の症例で思春期の発来が遅れるようだが，妊孕性に問題はない．

MRI検査では多くの症例で下垂体前葉低形成が観察され，これは下垂体ソマトトロフ細胞の低形成の反映と考えられる．しかし，報告例の多くは6歳以降の症例であり，出生時または乳児期から下垂体低形成が観察されるか否かは不明である．自験例では2歳時にMRIを施行しており，この時点では下垂体低形成は明らかではなかった[19]．

GH補充療法を開始した後の成長は良好であり，GH治療によく反応する．GH抗体の出現に関する報告はなく，適切な時期に治療を行えば目標身長への到達が期待できる．

5 臨床症例

筆者らが経験したGHRH受容体異常症を紹介する[19]．

【症例】初診時2歳3カ月，女児

【経過】妊娠・分娩経過に異常なく，在胎38週に頭位・自然分娩にて出生．出生時体重3,236g，身長50.0cm，頭囲33.0cm．1歳半健診で低身長を指摘され，以後も徐々に低身長が著明となり当院へ紹介された（図1a）．精神運動発達は正常であ

った.

【既往歴】特記事項なし.

【家族歴】父 169.5cm, 母 156cm, 兄 (4歳) 身長 +0.5SD. 血族婚なし.

【身体所見】身長 77.2cm (-3.1SD), 体重 8.9kg (肥満度 0%), 頭囲 44.0cm (-2.1SD). 軽度の前額部突出を認める.

【内分泌検査所見】IGF-1 7ng/mL, IGFBP-3 0.41μg/mL, TSH 3.73μIU/mL, FT3 3.75pg/mL, FT4 1.16ng/dL.

GH分泌刺激試験:

インスリン負荷:GH前値 0.27ng/mL, 頂値 2.81ng/mL

アルギニン負荷:GH前値 2.05ng/mL, 頂値 3.78ng/mL

GHRH負荷:GH前値 0.64ng/mL, 頂値 3.93ng/mL

【頭部MRI】下垂体高は 3mm で正常範囲内 (図 1b).

【遺伝子解析】*GH-1* に変異を認めなかったため, *GHRHR* の解析を行った. その結果, G136V と IVS2+3a>g の複合ヘテロ接合体変異を同定した. 両親の遺伝子解析の結果, G136V は父親由来, IVS2+3a>g は母親由来と判明した. G136V は GHRH 受容体の第1膜貫通領域にあり, 機能解析にて変異受容体では GHRH に対する cAMP の反応を認めなかった. また, IVS2+3a>g は mini-gene を用いたスプライスアッセイにより, 異常スプライスをきたすことが示唆された. すなわち, IVS2+3a>g により正常スプライスドナー部位の機能はほぼ完全に損なわれ, イントロン2が保持された転写産物が増加, またはより下流での cryptic splice site activation が起こりフレームシフトが起きると予想された.

【経過】GH補充療法に対する反応は良好であった (図 1a).

6 まとめ

GHRH受容体異常症は, 遺伝性IGHDタイプIBの表現型を示す稀な疾患である. 生後の早い段階から成長障害を示す重度のIGHDで, 異所性後葉や下垂体茎断裂を認めない場合は, *GH-1* または *GHRHR* 変異の検索の適応と考えられる. 自験例で認められたGH反応性の残存や, 下垂体サイズの保持が, 幼少期に限って認められる所見なのか否かの検討が, 今後の課題である.

文　献

1) Lindsay R et al : J Pediatr 125 : 29, 1994.
2) Vimpani GV et al : Br Med J 2 (6084) : 427, 1977.
3) Rona RJ et al : Arch Dis Child 52 : 197, 1977.
4) Cogan JD et al : Adv Pediatr 45 : 337, 1998.
5) Mayo KE et al : Recent Prog Horm Res 55 : 237, 2000.
6) Pombo CM et al : Endocrinology 141 : 2113, 2000.
7) Gaylinn BD : Receptors Channels 8 : 155, 2002.
8) Godfrey P et al : Nat Genet 4 : 227, 1993.
9) Lin SC et al : Nature 364 : 208, 1993.
10) Wajnrajch MP et al : Nat Genet 12 : 88, 1996.
11) Maheshwari HG et al : J Clin Endocrinol Metab 83 : 4065, 1998.
12) Netchine I et al : J Clin Endocrinol Metab 83 : 432, 1998.
13) Wajnrajch MP et al : Am J Med Genet A 120A : 77, 2003.
14) Salvatori R et al : J Clin Endocrinol Metab 84 : 917, 1999.
15) Alatzoglou KS et al : J Clin Endocrinol Metab 94 : 3191, 2009.
16) de Graaff LC et al : Clin Endocrinol (Oxf) 70 : 742, 2009.
17) 堀川玲子：日本臨牀 60 : 297, 2002.
18) Inoue H et al : Clin Endocrinol (Oxf) 74 : 223, 2011.
19) Soneda A et al : Growth Horm IGF Res 23 : 89, 2013.
20) Barreto-Filho JA et al : J Clin Endocrinol Metab 87 : 2018, 2002.